

Article

# Improvement of the Thermal and Mechanical Strength of the Starting Cage of Double-Cage Induction Motors

Jan Mróz <sup>1,\*</sup>  and Wojciech Poprawski <sup>2</sup>

<sup>1</sup> The Faculty of Electrical and Computer Engineering, Rzeszow University of Technology, Aleja Powstańców Warszawy 12, 35-959 Rzeszów, Poland

<sup>2</sup> Independent Researcher, 35-959 Rzeszów, Poland; w.poprawski@hotmail.com

\* Correspondence: janmroz@prz.edu.pl; Tel.: +48-178651360

Received: 25 October 2019; Accepted: 27 November 2019; Published: 29 November 2019



**Abstract:** This article discusses the thermal and mechanical exposure of the starting cage of a double-cage induction motor rotor during start-up. Damage to the starting cage is the most common cause of failure of a double-cage winding during long start-ups. It has been indicated that the end region of the double-cage winding is a key area in the search for a more damage-resistant solution. Among the available studies on improving the mechanical strength of double-cage windings, which typically focuses on improving the cooling system, modifying the shape of the slots, or altering the bar material, a new concept of improving the mechanical strength through the modification of the structure of the end region has appeared. This is achieved by applying sleeves onto the ends of the starting cage bars, which helps to reduce the temperature of the connection between the starting bars and the end rings. A simulation of the temperature field of a double-cage induction motor with this new design is performed and discussed in this paper. It has been confirmed that the new design solution effectively improves the mechanical strength of the starting cage, making it less prone to damage caused by thermal stresses.

**Keywords:** double-cage induction motor; improvement of motor reliability; cage winding constructions; direct start-up; coupled electromagnetic-thermal model

## 1. Introduction

In a cage induction motor with an emergency locked rotor, or under long starting conditions, the element most vulnerable to damage is the cage winding of the rotor. Thermal exposure is particularly high in double-cage rotor motors owing to the relatively low thermal capacity of the starting cage bars. Such motors are typically found in drives requiring high starting torque, which translates directly into higher losses in the starting cage. Examples of damage to the starting cage in double-cage motors are displayed in Figures 1 and 2. The most common cause of double-cage winding failure is damage to the starting cage, while the working cage remains functional. This is a defect that is difficult to detect in its initial phase. There are numerous publications presenting new approaches to detecting starting cage failures in a double-cage motor. Thus, [1] presents a method of detecting outer cage damage in double squirrel cage induction motors. This diagnostic method relies on a discrete wavelet transform optimised for sensitive detection under transient operating conditions. Reference [2] presents a complete on-line condition monitoring system designed to detect incipient broken rotor bar faults in a double-cage induction motor using the stator current signature. It is based on successful combination of one of the latest variants of wavelet techniques, the recursive stationary wavelet packet transform and a tool widely used in quality control, the statistical process control in order to deal with

several challenges in the continuous monitoring of the incipient fault. In [3] the possibility of using the stator phase current waveform as a diagnostic signal to detect faults in a double squirrel cage induction motor is discussed. On the basis of tests conducted on a double cage motor prototype, conditions were formulated for distinguishing faults in cages of both medium and high power machines.



**Figure 1.** Damaged rotor cage, view after cutting off the end ring of the starting cage—visible melting of the starting cage bar.



**Figure 2.** Damaged rotor cage—visible sheared bars of the starting cage.

An important, developing issue is diagnosing large induction motors fed by an inverter. Reference [4] presents the use of a fuzzy-based statistical feature extraction from the air gap disturbances for diagnosing broken rotor bars in large induction motors fed by line or an inverter. The method is based on the analysis of the magnetic flux density variation in a Hall Effect Sensor installed between two stator slots of the motor. Reference [5] provides a diagnosis of broken rotor bars in field oriented controlled double cage induction motors, based on current and vibration signature analysis techniques.

Designers and constructors are making attempts to make the double-cage winding more resistant to damage occurring during long start-ups. One of the lines of action is to improve the cooling system. In [6] the cooling performance of axial fans with forward-swept and inclined blades and a structure with low ventilation resistance in large-capacity open-type motors is studied.

Steps are taken for thermal analysis to be more deeply regarded in electric machine design. In [7] some of these problems are discussed and advice is provided as to dealing with them when developing algorithms for inclusion in design software. In [8], a design of a 115 kW squirrel cage induction motor

for electric vehicle applications is presented. In the design procedure, initially, an analytical design of the electric vehicle motor is performed depending on specific design criteria. Then, the analytical design is verified by means of finite element analysis. Reference [9] presents the coupled fluid-thermal analysis for an induction motor with healthy and broken bar rotors. Much attention was paid to developing the fluid model on the basis of the computational fluid dynamic theory.

Another area of work aimed at improving the fault resistance of the double cage winding and the deep bar rotor to the effects of a prolonged start-up focuses on changing the cage winding material and modifying the shape of rotor slots. In [10] three double-cage induction motors have been simulated and their electromagnetic characteristics compared. The study is carried out using finite element method (FEM) analysis. Reference [11] presents dynamic modelling of a series of induction motor squirrel cages with different shapes of rotor deep bars, taking into account the skin effect. Reference [12] focuses on designing and optimizing an induction motor with a lower cost and high performance. The starting torque of the induction motor, which is an important aspect in traction applications, has been improved by applying a rotor with a double cage. Analytical modelling is carried out and it is validated by means of FEM analysis. In [13] a new design of the rotor bar which allows to improve the starting torque without decreasing motor efficiency is presented. Reference [14] deals with the influence of the shape of the cage on double cage induction motor's parameters, mainly the values of starting torque, breakdown torque, as well as the power factor, efficiency and starting current. The optimal shape of the rotor slot has been identified for the maximum size of the relative starting torque and minimum size of the relative starting current while maintaining a favorable power factor and efficiency of the motor.

Another area of work undertaken by constructors to improve the fault resistance of the cage winding are special motor structure designs. In [15] an investigation on the design of a high-power induction motor with special constraints is presented. Direct online start-up and pull-up torque of high value are the two imposed requirements. The proposed solution advances a new rotor structure with two different rotor cages. Reference [16] presents the elaborate design procedure for a double rotor double cage motor. The two rotors can run independently, at an equal or unequal speed, depending on their individual loading.

In [17,18], using mathematical models to consider the electromagnetic and thermal interrelations, the author demonstrated that the end region of the cage is a key location in the search for construction solutions more resistant to damage. These were likely the inspiration for the construction of the starting cage of a double-cage motor as discussed in [19], which, according to the authors, allows for a reduction of the temperature of the end region of the starting cage bars. This is achieved by applying sleeves onto the ends of the starting cage bars. Because [19] does not present any test results for a motor with a double-cage winding constructed in such a manner, it is necessary to test the effectivity of this new design. The aim of the present paper is to perform a simulation of the temperature field of a double-cage induction motor with the new construction solution of the starting cage, during start-up with a locked rotor. The results are compared with those of a motor with a starting cage of conventional structure. All results presented in this paper have been achieved through a simulation and should be verified through experimental research in the future. The problem of experimental research on high-powered motors is related to a number of logistic activities, as they typically must be performed under industrial conditions. This entails high experimental costs. Therefore, there are relatively few publications addressing experimental research related to the heating of high-power cage induction motors [20–22].

## 2. Method of Analysing the Temperature Field of a Double-Cage Induction Motor

The analysis of thermal and electromagnetic phenomena occurring in an induction motor is commonly conducted by means of professional software available on the market. There are many publications on this issue [6,8,9,12,23]. A considerable limitation, particularly at an early stage of work on the presented problem, is the cost and a long calculation time for 3D issues, hence the choice of faster and less expensive methods which have been partially verified through experimental research [17,24].

Reference [17] presents a mathematical model and corresponding 3D simulation model that allows the determination of the temperature field of a double-cage motor in transient electromechanical states. It uses a heat network created by the control volume method [25]. The model considers mutual electromagnetic and thermal dependencies. Because the dynamics of electromechanical phenomena in electric machines are considerably greater than those of thermal phenomena, an electromechanical problem can be solved at a specific moment and for a given temperature field. In the next time step, a new temperature field can be calculated using the solution of the electromechanical problem from the previous time step. This procedure is presented in the block diagram in Figure 3.

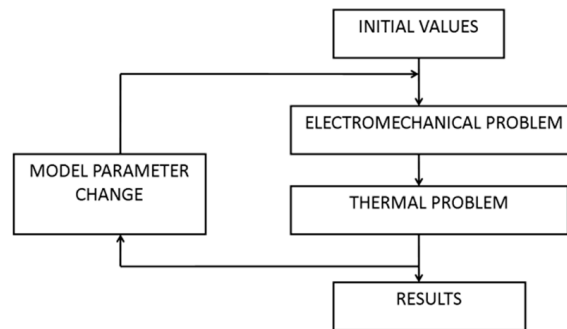


**Figure 3.** Algorithm for calculating rotor thermal field.

The motor model used in calculations is designed for simulations of short operation periods (operating with a locked rotor or during start-up). Research shows that under those operating conditions the heating of the stator components may be examined regardless of the rotor heating [17,24]. The operation periods analysed here are too short for the stator to exert a noticeable influence on the rotor heating and vice versa. Therefore, the heat exchange between the stator and the rotor can be omitted in the analysis. The temperature field is calculated for the area indicated in Figure 4, which encompasses a half of the rotor's length and half of the rotor's slot pitch. The analysed area has three types of boundary conditions: the Dirichlet boundary condition for the  $A_1$  surface, the Neumann condition for the  $A_2$ ,  $A_3$ , and  $A_4$  surfaces, and the Newton condition for the areas that are in direct contact with a cooling fluid.

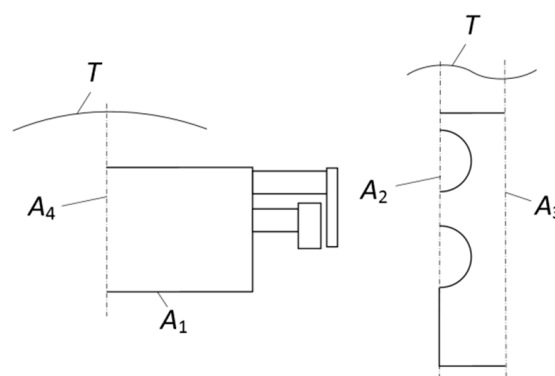


**Figure 4.** Analysed area of double-cage motor's rotor.

In the control volume method, the analysed object is subdivided into a number of homogeneous elements. The energy balance is calculated for the entire system. If it is assumed that in the analysed object, the separate control element with volume  $V_{c(i)}$  is sufficiently small that the temperature in its entire area is the same and has the value  $T_{(i)}$ , and that the point heat source  $\dot{q}_{V(i)}$  is located at the centre of gravity of this element, then the transient temperature field in a motor analysed using the heat

network created by the control volume method [25] is described by the following system of Equation (1) together with the initial condition (2):

$$\sum_j \Lambda_{(i,j)} T_{(j)} - \left( \sum_m \Lambda_{a(i,m)} + \sum_j \Lambda_{(i,j)} \right) T_{(i)} + \sum_m \Lambda_{a(i,m)} T_{a(i)} + V_{c(i)} \dot{q}_{v(i)} = V_{c(i)} c_{(i)} \rho_{(i)} \frac{dT_{(i)}}{dt}, \quad (1)$$

where  $i = 1, 2, \dots, z_n$  is the number of elements into which the considered area is divided,  $z_n$  is the number of area elements,  $\Lambda_{(i,j)}$  is the thermal conductivity for the heat flowing from node  $i$  to node  $j$ ,  $\Lambda_{a(i,m)}$  is the thermal conductivity for the heat flowing from node  $i$  to the external surface  $m$  and the heat transferred from surface  $m$ ,  $c$  is the specific heat,  $\rho$  is the density,  $t$  is the time,  $\dot{q}_{v(i)}$  is the volumetric density of the heat sources, and  $T$  is the temperature:

$$T(\mathbf{r}, t)|_{t=0} = T_0(\mathbf{r}), \quad (2)$$

where  $T_0$  is the initial temperature and  $\mathbf{r}$  is the positional vector describing the position of the element in question. To determine  $\dot{q}_v$  in the area of the windings, it is necessary to calculate the distribution of the current density  $J(\mathbf{r}, t)$ . Then:

$$\dot{q}_v = J^2(\mathbf{r}, t) \frac{1}{\gamma(T)}, \quad (3)$$

where  $\gamma$ -conductivity.

For a double-cage induction motor with a soldered cage, the equations describing the transient electromechanical state in a two-axis coordinate system rotating at the speed  $\omega_x$  have the form [26]:

$$\mathbf{U} = \frac{d}{dt} \Psi + \Omega \Psi + \mathbf{R} \mathbf{I}, \quad (4)$$

$$\Psi = \mathbf{L} \mathbf{I}, \quad (5)$$

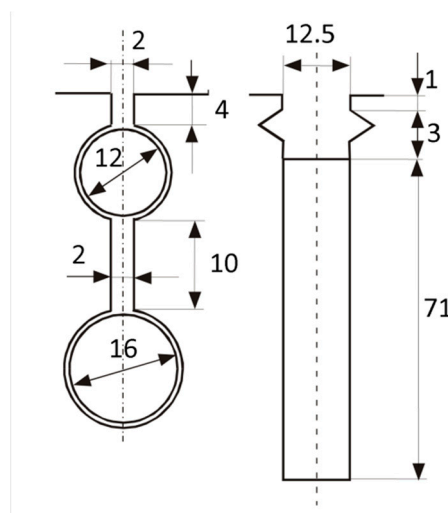
$$J_m \frac{1}{p} \frac{d\omega}{dt} = p \operatorname{Re}(j \underline{\Psi}_1 I_1^*) - T_L \quad (6)$$

where  $\mathbf{U} = [\underline{U}_1, 0, 0]^T$ ,  $\mathbf{I} = [I_1, I_{2(1)}, I_{2(2)}]^T$ , and  $\Psi = [\underline{\Psi}_1, \underline{\Psi}_{2(1)}, \underline{\Psi}_{2(2)}]^T$  are the voltages, currents, and linkage fluxes, respectively,  $\Omega = \operatorname{diag}[j\omega_x, j(\omega_x - \omega), j(\omega_x - \omega)]^T$ ,  $\mathbf{R}$  and  $\mathbf{L}$  are the resistance and inductance matrices,  $\omega$  is the electric rotor angular velocity,  $U_1$  is the amplitude of the supply voltage,  $I_1$ ,  $I_{2(1)}$ , and  $I_{2(2)}$  are the stator and rotor two-axis vector currents (complexor), respectively,  $J_m$  is the moment of inertia,  $T_L$  is the load torque, and  $p$  is the number of pole pairs. Knowledge of the currents flowing in the motor windings allows the determination the volumetric density of heat sources  $\dot{q}_V$  necessary to determine the temperature field of the motor winding. This method allows the calculation of the temperature field for the double-cage induction motor with the parameters presented in Table 1.

**Table 1.** Chosen motor parameters.

Parameter	Value
Rated power, kW	320
Rated voltage, V	6000
Rated frequency, Hz	50
Number of pole pairs	3
Air gap, mm	1.6
Stator diameter, m	0.888/0.600
Rotor diameter, m	0.597/0.369
Core length, m	0.56
Number of stator/rotor slots	72/58
Class of insulation	F
Ratio of coil span to pole pitch	10/12
Number of stator—winding turns per phase	240
Stator—winding resistance, $\Omega$	0.648

The winding of the cage consists of bars short-circuited with copper end rings. The bars of the starting cage are made of brass, whereas the bars of the working cage are made of copper. The dimensions of the rotor and stator slots are shown in Figure 5.

**Figure 5.** The shape and dimensions of rotor and stator slots of double-cage motor with a welded cage.

The heat transfer coefficient from the areas in direct contact with cooling air was calculated on the basis of paper [18]. It provides an equation for calculating the equivalent heat transfer coefficient through natural convection and radiation, in the following form:

$$\alpha = \nu_p K_p (T + T_0) (T^2 + T_0^2) + C_k \sqrt{\phi} (T - T_0)^{0.25}, \quad (7)$$

where:  $\nu_p$  is the emissivity coefficient of the surface,  $K_p$  is the Boltzman constant,  $T$  is the surface temperature,  $T_0$  is the temperature of the air surrounding the surface,  $C_k$  is the coefficient included within the limits (2.79 ... 3.39)  $\text{W/m}^2\text{K}$ ,  $\phi$  is the relative air humidity. For  $T = 300 \text{ }^\circ\text{C}$ ,  $T_0 = 20 \text{ }^\circ\text{C}$ ,  $\phi = 0.9$ ,  $\nu_p = 0.85$  (varnished surface),  $C_k = 3 \text{ W/m}^2\text{K}^{1.25}$  the heat transfer coefficient is  $\alpha = 13.2 \text{ W/m}^2\text{K}$ . For a rotating rotor (forced convection):

$$\alpha_v = \alpha (1 + k \sqrt{v}), \quad (8)$$

where  $v$  is the speed of the cooling air thrown over the surface,  $k$  the coefficient included within the range 0.5 ... 1.3, in the analysis  $k = 1$  was assumed for the end region. For the rated speed:  $\alpha_v = 58 \text{ W/m}^2\text{K}$ .

Thermal conductivity values: for the bars of the working cage 372 W/m·K, for the end rings of the working cage 372 W/m·K, for the bars of the starting cage 103 W/m·K, for the end rings of the starting cage 372 W/m·K. For the rotor core—50 W/m·K (in axial direction), 10 W/m·K (in radial direction). A slight change due to the temperature of the thermal conductivity coefficient was omitted (within the expected temperature range within 20 ... 400 °C).

### 3. Influence of the End Region Structure of the Double-Cage Winding on Mechanical Stresses

In a double-cage motor with a soldered cage, the mechanical stresses associated with the skin effect in the rotor bars are not as important as in a deep bar motor. In a double-cage winding, the forces due to the thermal expansion of the end ring and centrifugal forces originating from the mass of the end region of the winding are more significant. The associated stresses can be dangerous, especially during long start-up periods, when the end rings experience maximum heat.

In double-cage motors with a soldered winding, the end rings are typically moved away from the core. There are many construction solutions for soldered bar connections with rings. Insert connections, as displayed in Figure 6, are frequently used.

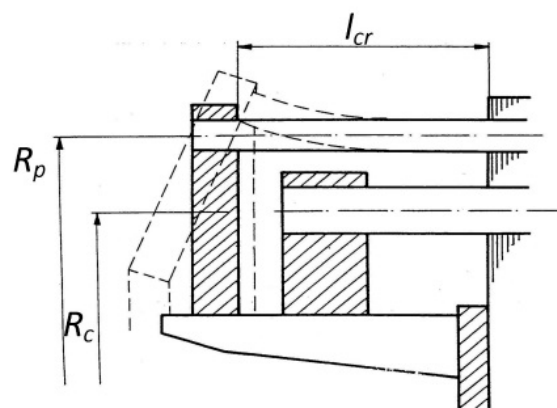


Figure 6. Insert connections in double-cage motor.

The length of the overhang of the bars beyond the core is limited mainly by implementation considerations. An excessive increase of the overhang is meaningless owing to the length of the entire machine. This problem was discussed, among others, in [18]. The model of the phenomena occurring in the external heated part, rotating at a constant winding speed, assumes that the bar is rigidly fixed in the packet, and a radial force and circular-symmetric moment act in the location of the rigid connection of the bar to the ring. They cause the displacement of the external part of the cage as indicated by the dashed line in Figure 6. During the motor start-up, the centrifugal forces and forces originating from the thermal deformations of the ring act together on the cage bars.

Using this model, simulation calculations were conducted for a double-cage induction motor with parameters presented in Table 1. The results are presented in Figure 7 as the total stress value in the bars during a prolonged motor start-up.

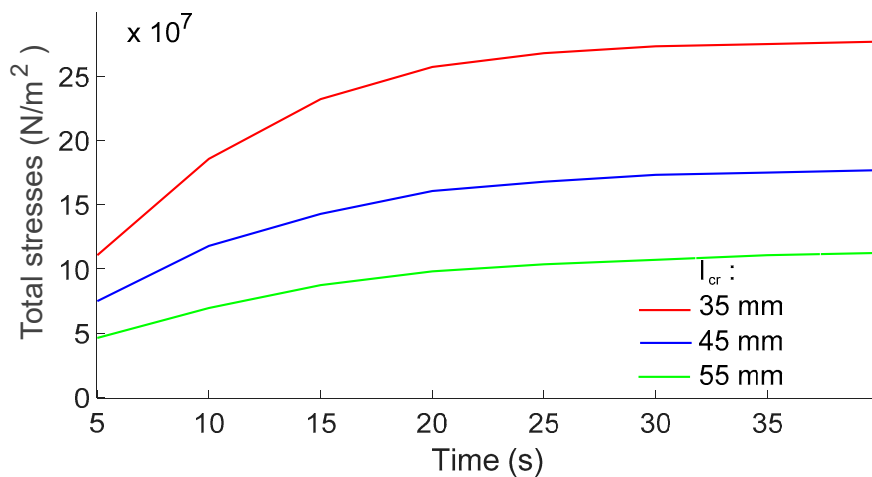
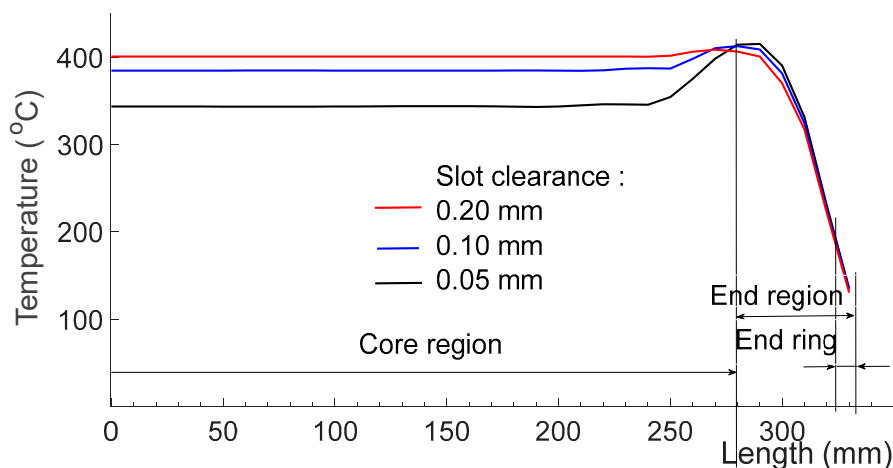


Figure 7. Stresses in starting-cage bar during motor start-up.

As can be observed in Figure 7, a change in the outward extension of the bars within the limits of 23% around the value of  $l_{cr} = 45$  mm causes a significant change in the total stresses when the bar emerges from the core during a long-term startup. When reducing the size of  $l_{cr}$ , the stress increases by approximately 56%; when the value of  $l_{cr}$  increases, the stresses decrease by approximately 36%. In double-cage motors with bars of a circular cross section, the highest temperature occurs in the end part of the cage. The natural method to avoid a large unevenness in temperature distribution along the bar would be to eliminate the areas with elevated temperature from the cage structure, i.e., to shorten the bars. However, the reduction of this overhang leads to a significant increase in the mechanical stresses in the bars due to the thermal deformations of the end ring.

#### 4. Possibilities of Equalising the Temperature Distribution along the Axis of the Motor Starting Cage Bar

In certain cases, the temperature in the end region of the cage is sufficiently high to cause a loss of elasticity of the material, whereas in the remainder of the winding, the temperature does not significantly reduce the mechanical strength of the bar material. These highly heated end regions of the rotor winding determine the durability and reliability of the entire motor, despite the fact that their share in the volume of the cage is small. Therefore, we must attempt to obtain a more uniformly heated structure. This applies, in particular, to work in conditions of prolonged start-up or operation with a locked rotor. This issue is discussed in [18], where the possibilities of equalising the temperature distribution along the axis of the starting cage bar of a double-cage motor were considered. The influence of the slot clearance was examined (Figure 8) for a double-cage induction motor with parameters presented in Table 1. The conditions of the heat transfer from these parts to the temperature field of the cage, in the state of working with the rotor locked, were also examined (Figure 9).



**Figure 8.** Influence of slot clearance on temperature distribution along starting-cage bar.

Figure 8 displays the temperature distribution along the starting cage bar with different fits of the bar to the slot (slot clearance 50, 100 or 200  $\mu\text{m}$ ). From the calculation results displayed in Figure 8, it can be observed that improving the fit of the bar to the slot leads to a significant reduction in the bar temperature in the core part; however, the temperature remains high in the end region and this costly treatment does not eliminate the cage damage discussed above. Because only somewhat exceeding a certain temperature (dependent on the bar material) decreases the tensile strength sharply, even a marginal reduction in the temperature of the end regions is beneficial from the point of view of its durability. To obtain similar conditions for heat exchange in the end region and slot part of the cage, an equality of thermal resistance should be ensured by means of heat transfer between the external part of the bar and the surrounding air, and between the cage bar and the rotor core. For the motor considered, the value of the heat transfer coefficient in the external parts of the cage was calculated, providing heat transfer conditions similar to those in the slot part, i.e.,  $254 \text{ W/m}^2\text{K}$ . The temperature distribution along the bars of the starting cage after 12 s of operation of the motor with the rotor locked supplied with the rated voltage is displayed in Figure 9. It is not possible to obtain a coefficient of this value in ordinary construction solutions because the values of this coefficient encountered in practice are many times smaller than required.

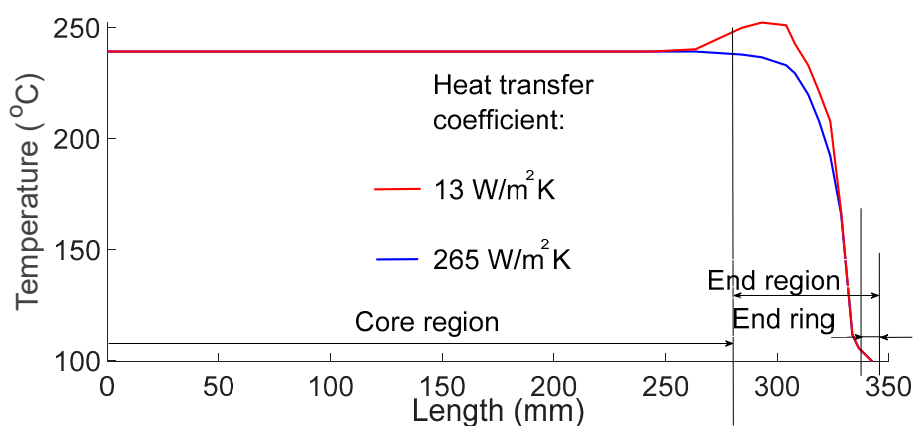


**Figure 9.** Influence of heat of transfer coefficient from end region of cage to temperature distribution along bar axis.

## 5. New Solution for the Construction of a Starting Cage of a Double-Cage Motor

The presented review of the results of calculations of the temperature of the double-cage winding indicates that in the end region of the cage construction, the possibility of further increasing the

resistance of the cage to the related effects of working with the locked rotor and during a prolonged start-up should be investigated. The end region of the starting cage is most exposed to destructive activities under these working conditions, and it is necessary to investigate the possibility of increasing the resistance of the double-cage winding to the effects of a prolonged start-up.

The authors of [19] presented a proposal for an innovative construction solution of the starting cage that allows a limitation of the temperature of the end region of the bars. The starting cage displayed in Figure 10, based on this solution, is characterised by sleeves (3) of the same material as the bars, applied to the ends of all the bars (1) protruding from the core. The sleeves (3) adjacent to the end rings (2) are preferably permanently connected to the rings using a hard solder, welding, or sealing.

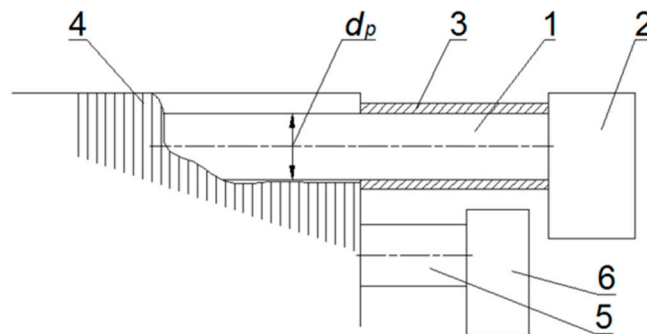


**Figure 10.** Innovative construction solution of starting cage: 1—starting cage bar, 2—end ring of starting cage, 3—sleeve, 4—core, 5—working cage bar, 6—end ring of working cage,  $d_p$ —diameter of starting bar.

The method of building the starting cage is based on the fact that after inserting the bars (1) into the slots, the sleeves (3) are heated to a temperature at which the inner diameter of the sleeve is larger than the diameter of the bar  $d_p$ . Before the sleeves are heated, the inner diameter of the sleeve  $d_r$  is less than the diameter of the rotor cage bar. Then, the hot sleeves (3) are applied to the ends of the bars (1). Finally, to the ends of the bars (1), the end rings (2) are inserted and joined with the bars and sleeves with hard solder, welding, or sealing.

The sleeves (3) superimposed on the ends of the bars (1) increase the cross section and thermal capacity of the external part of the bars (1); thus, in the ends of the bars (1), the current density is reduced and the temperature decreases. Hence, a starting cage prepared in this manner is characterised by greater start-up durability.

## 6. Simulation Tests of the Temperature Field of a Double-Cage Motor with a New Design Solution

Using Equations (1)–(6), simulation tests were performed for a double-cage motor with the parameters presented in Table 1, with an emergency locked rotor ( $\omega = 0$ ). The calculations were performed for both a motor with a starting cage of conventional structure and a double-cage induction motor with the new construction solution for the starting cage presented in [19].

Figure 11 displays the temperature distribution along the centre axis of the starting cage bar for the classic solution and with 1.8 mm thick sleeves made of brass, similar to the starting cage bars. Figure 12 indicates the influence of the thickness of the sleeves (1.8 mm and 1.0 mm) on the distribution of the temperature along the axis of the starting cage bar. Owing to the new construction of the end region of the starting cage, locations previously threatened by overheating are largely eliminated. For the solution proposed in [19], the temperature of the starting bar in the region of the outward reach of the bars is considerably less than for the classical solution. Increasing the thickness of the sleeves further reduces this temperature (Figure 12).

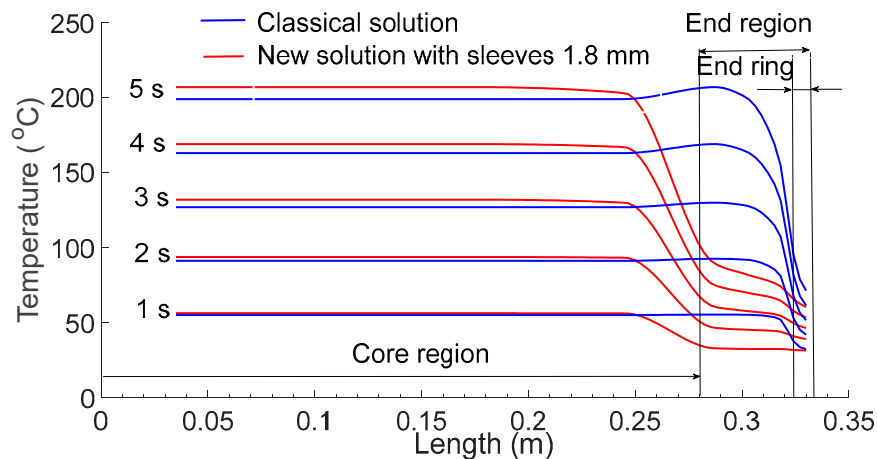


**Figure 11.** Distribution of temperature along axis of starting-cage bar for classic solution and with sleeves.

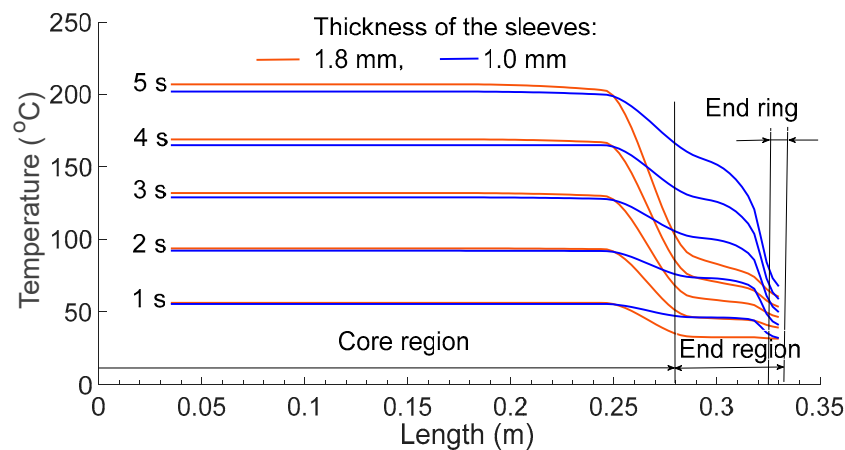


**Figure 12.** Influence of thickness of sleeves on temperature distribution along axis of starting-cage bar.

## 7. Conclusions

The startup process of the induction cage motor is one of the most important phases of the drive operation. During the start-up an electrical motor can be subject to severe electrical and thermal loads. These loads, despite their relatively short durations, significantly affect the motor's lifetime and reliability. The heat generated during a prolonged start-up causes mechanical stresses which may damage the motor cage. By using the double-squirrel-cage soldered winding, large values of starting torques are achieved. This is, however, at the cost of non-uniform heating of the cage, along with the tendency of the cage bars to overheat. A large amount of heat is released during start-up in the bars of the motor's starting cage. The highest temperature is observed in the end region of the starting cage bar. There is a significant difference in the axial temperature distribution in the bars owing to the different types of heat exchange in the core region and the end region of the bars. The limitation of the slot clearance to improve heat transfer into the core does not change the fact that the temperature of the end region of the bars remains high. Moreover, reducing the distance between the end rings and the core is disadvantageous owing to the increase in the bending stress in the bars from the thermal expansion of the rings. Excessive heating of the end region of the starting cage during start-up can lead to motor failure.

The application of sleeves onto the ends of the starting cage bars can significantly reduce the temperature of the connection of the starting cage bars with the rings and thus increase the resistance of the rotor starting cage to thermal exposure during motor start-up. The conducted simulation tests demonstrated that thanks to the new construction of the end region of the starting

cage, locations previously threatened by overheating were largely eliminated. However, there arise additional technological difficulties associated with the process of setting the sleeves onto the bars of the starting cage.

The heating of the motor windings is a transient phenomenon which is closely related to the transient electromechanical process. Both processes are mutually related since the distribution of heat sources depends on the temperature of motor windings. The results of the analysis can be massively improved by applying detailed numeric calculation methods (FEM analysis). A considerable limitation, particularly at an early stage of work on the presented problem, is the cost and a long calculation time for 3D coupled problems, hence the choice of faster and less expensive methods which have been partially verified through experimental research.

In view of the relatively limited number of publications in the area of costly experimental research involving high-power motors, it is necessary to plan and conduct such research. This applies in particular to investigating energy aspects in transient states for verifying the simulation models and the further improvement of cage winding constructions.

**Author Contributions:** Conceptualization, J.M. and W.P.; methodology, J.M.; software, J.M.; formal analysis, J.M. and W.P.; investigation, J.M. and W.P.; resources, J.M.; writing—original draft preparation, J.M.; writing—review and editing, J.M. and W.P.; visualization, J.M.; supervision, J.M.; project administration, J.M.; funding acquisition, J.M.

**Funding:** This work is financed in part by the statutory funds of the Department of Electrodynamics and Electrical Machine Systems, Rzeszow University of Technology and in the part by Polish Ministry of Science and Higher Education under the program “Regional Initiative of Excellence” in 2019–2022. Project number 027/RID/2018/19, amount granted 11 999 900 PLN.

**Conflicts of Interest:** The authors declare no conflict of interest.

## References

1. Gritli, Y.; Lee, S.B.; Filippetti, F.; Zarri, L. Advanced diagnosis of outer cage damage in double-squirrel-cage induction motors under time-varying conditions based on wavelet analysis. *IEEE Trans. Ind. Appl.* **2014**, *50*, 1791–1800. [[CrossRef](#)]
2. Hmida, M.A.; Braham, A. An on-line condition monitoring system for incipient fault detection in double-cage induction motor. *IEEE Trans. Instrum. Meas.* **2018**, *67*, 1850–1858. [[CrossRef](#)]
3. Tulicki, J.; Weireb, K.; Sulowicz, M. The possibility of distinguishing rotor cage bar faults in double squirrel cage induction motors on the basis of the stator current signal. In Proceedings of the 2017 International Symposium on Electrical Machines (SME), Naleczow, Poland, 18–21 June 2017.
4. Dias, C.G.; da Silva, L.C.; Chabu, I.E. Fuzzy-based statistical feature extraction for detecting broken rotor bars in line-fed and inverter-fed induction motors. *Energies* **2019**, *12*, 2381. [[CrossRef](#)]
5. Gritli, Y.; Tommaso, O.D.I.; Miceli, R.; Filippetti, F.; Rossi, C. Vibration signature analysis for rotor broken bar diagnosis in double cage induction motor drives. In Proceedings of the 4th International Conference on Power Engineering, Energy and Electrical Drives, Istanbul, Turkey, 13–17 May 2013; pp. 1814–1820.
6. Nakahama, T.; Biswas, D.; Kawano, K.; Ishibashi, F. Improved cooling performance of large motors using fans. *IEEE Trans. Energy Convers.* **2006**, *21*, 324–331. [[CrossRef](#)]
7. Staton, D.; Boglietti, A.; Cavagnino, A. Solving the more difficult aspects of electric motor thermal analysis in small and medium size industrial induction motors. *IEEE Trans. Energy Convers.* **2005**, *20*, 620–628. [[CrossRef](#)]
8. Ulu, C.; Korman, O.; Komurgoz, G. Electromagnetic and thermal design/analysis of an induction motor for electric vehicles. In Proceedings of the 2017 8th International Conference on Mechanical and Aerospace Engineering (ICMAE), Prague, Czech Republic, 22–27 July 2017.
9. Xie, Y.; Guo, J.; Chen, P.; Li, Z. Coupled fluid-thermal analysis for induction motors with broken bars operating under the rated load. *Energies* **2018**, *11*, 2024. [[CrossRef](#)]
10. Gyftakis, K.N.; Athanasopoulos, D.; Kappatou, J. Study of double cage induction motors with different rotor bar materials. In Proceedings of the 20th International Conference on Electrical Machines (ICEM), Marseille, France, 2–5 September 2012; pp. 1450–1456.

11. Maddi, Z.; Aouzellag, D. Dynamic modelling of induction motor squirrel cage for different shapes of rotor deep bars with estimation of the skin effect. *Prog. Electromagn. Res.* **2017**, *59*, 147–160. [[CrossRef](#)]
12. Sundaram, M.; Mohanraj, M.; Varunraj, P.; Kumar, T.D.; Sharma, S. FEA based electromagnetic analysis of induction motor rotor bars with improved starting torque for traction applications. In Proceedings of the International Conference on Automatic Control, Mechatronics and Industrial Engineering (ACMIE), Suzhou, China, 29–31 October 2018.
13. Lee, H.J.; Im, S.H.; Um, D.Y.; Park, G.S. A design of rotor bar for improving starting torque by analyzing rotor resistance and reactance in squirrel cage induction motor. *IEEE Trans. Magn.* **2017**, *99*, 1–4. [[CrossRef](#)]
14. Orsag, O.; Rusnok, S.; Sobota, P.; Kacor, P. Influence of rotor slot on the parameters of induction motor. In Proceedings of the 2017 IEEE International Conference on Environment and Electrical Engineering and 2017 IEEE Industrial and Commercial Power Systems Europe (EEEIC/ICPS Europe), Milan, Italy, 6–9 June 2017.
15. Livadaru, L.; Simion, A.; Munteanu, A.; Cojan, M.; Dabija, O. Dual cage high power induction motor with direct start-up design and FEM analysis. *Adv. Electr. Comput. Eng.* **2013**, *13*, 55–58. [[CrossRef](#)]
16. Sinha, S.; Deb, N.K.; Biswas, S.K. The design and its verification of the double rotor double cage induction motor. *J. Inst. Eng. (India) Ser. B* **2017**, *98*, 107–113. [[CrossRef](#)]
17. Mróz, J. *The Analysis of Coupled Electromechanical and Thermal Problems in Transient States of Double-Cage Induction Motors*; Publishing House Rzeszow University of Technology: Rzeszow, Poland, 2013.
18. Mróz, J. Possibilities of equalizing the temperature distribution in the bars of the starting cage along the axis of a double cage induction motor. *Przełąd Elektrotech.* **1998**, *12*, 314–317.
19. Poprawski, W.; Wolnik, T. Innovative design of double squirrel cage induction motor for high start frequency operation. *Electr. Mach. Trans. J. Inst. Electr. Drives Mach. KOMEL* **2016**, *111*, 41–44.
20. Krok, R. Influence of work environment on thermal state of electric mine motors. *Arch. Electr. Eng.* **2011**, *60*, 357–370. [[CrossRef](#)]
21. Al' Akayshee, Q.; Staton, D.A. 1150 hp motor design, electromagnetic and thermal analysis. In Proceedings of the 15th International Conference on Electrical Machines (ICEM), Bruges, Belgium, 25–28 August 2002.
22. Dymond, J.H.; Ong, R.; Stranges, N. Instrumentation, testing, and analysis of electric machine rotor steady-state heating. *IEEE Trans. Ind. Appl.* **2002**, *38*, 1661–1667. [[CrossRef](#)]
23. Naderi, P. Modified magnetic-equivalent-circuit approach for various faults studying in saturable double-cage-induction machines. *IET Electr. Power Appl.* **2017**, *11*, 1224–1234. [[CrossRef](#)]
24. Mróz, J. The model of double-cage induction motor for the analysis of thermal fields in transient operations. *Arch. Electr. Eng.* **2017**, *66*, 397–408. [[CrossRef](#)]
25. Taler, J.; Duda, P. *Solving Straight and Reverse Problems of Heat Conduction*; WNT: Warsaw, Poland, 2003.
26. Paszek, W. *Transient States of AC Electric Machines*; WNT: Warsaw, Poland, 1986.

